

Effect of CuO chains on the local density of states in the vortex phase of $\text{YBa}_2\text{Cu}_3\text{O}_7$

W A Atkinson

Department of Physics and Astronomy, Trent University, 1600 West Bank Dr.,
Peterborough ON, K9J 7B8, Canada

E-mail: billatkinson@trentu.ca

Abstract. We examine the effects of the CuO chains on the density of states in the vortex phase in $\text{YBa}_2\text{Cu}_3\text{O}_7$, via a calculation based on the tight-binding proximity model. In this model, chain superconductivity results from single-electron hopping between the intrinsically-normal chains and intrinsically-superconducting CuO_2 planes. The calculations are based on self-consistent solutions of the Bogolyubov-de Gennes equations for a bilayer consisting of a single CuO_2 layer and a single CuO chain layer. We find that, in addition to the dispersing resonances found in single-layer models, the chains introduce a second set of dispersing resonances associated with the induced gap in the chain layer. These new resonances are highly anisotropic and distort the vortex core shape.

PACS numbers: 74.25.Jb,74.25.Qt,74.72.Bk

Submitted to: *Supercond. Sci. Technol.*

1. Introduction

Because of the availability of large high-quality single crystals, $\text{YBa}_2\text{Cu}_3\text{O}_{7-\delta}$ is one of the most widely studied of the high temperature superconductors (HTS). As with other HTS, the essential structural components are the two-dimensional (2D) CuO_2 layers. In these layers, the Cu and O orbitals are partially filled and are therefore conducting. The interlayer coupling is generally weak, meaning that the electronic bands contributing at the Fermi energy derive most of their weight from individual CuO_2 layers. For this reason, the standard model for a generic cuprate HTS consists of a single 2D CuO_2 layer in isolation.

$\text{YBa}_2\text{Cu}_3\text{O}_{7-\delta}$ differs from other cuprate HTS in one significant respect: in addition to the CuO_2 layers, there are layers of one-dimensional (1D) chains. Band structure calculations[1] suggest that the chains are roughly one-quarter filled, and contribute a quasi-1D Fermi surface. Despite this, the chains are nearly always ignored in theories of $\text{YBa}_2\text{Cu}_3\text{O}_{7-\delta}$, presumably because it has many physical properties that are common to all HTS, suggesting a minor role for the chains. In addition, the metallicity of the chains has been questioned, either because electrons in 1D are localized by arbitrarily weak disorder, or because they are unstable towards the formation of insulating charge density wave states.

Early evidence for the metallicity of the chains came from measurements of the resistivity anisotropy[2], which found $\rho_a/\rho_b \approx 2$ at 100 K, where ρ_a and ρ_b are the resistivities parallel to the two axes of the CuO_2 planes, and where b is also parallel to the chains. Such an anisotropy is expected if the chains are conducting and carry current in parallel with the planes. Since O-vacancies, which are prevalent in $\text{YBa}_2\text{Cu}_3\text{O}_{7-\delta}$, would strongly localize 1D electrons, the observed anisotropy appears to indicate a relatively large hybridization of chain and plane states. Further support for this comes from c -axis (perpendicular to the planes) resistivity measurements[3, 4] which find an anisotropy $\rho_c/\rho_a \approx 50$ at 100 K in optimally-doped $\text{YBa}_2\text{Cu}_3\text{O}_{6.93}$. In a tight binding model, this corresponds to $t_\perp/t \approx 7$ where t and t_\perp are the in-plane and perpendicular hopping amplitudes. This anisotropy is smaller than in other HTS and suggests coherent c -axis transport[5].

There has been some debate as to whether the CuO chains undergo a Peierls transition to a charge density wave state. Scanning tunneling microscopy (STM) experiments on chain-terminated surfaces found charge modulations which were interpreted as charge density waves.[6] However, later experiments[7] found that the modulation wavelength depends on the bias voltage of the STM tip, which is a characteristic of Friedel oscillations (i.e. standing wave patterns produced by impurity scattering of itinerant electrons) rather than charge density waves. These later experiments are consistent with metallic chains.

Direct evidence for a chain Fermi surface has recently been found in a number of angle resolved photoemission experiments[8, 9, 10]. The Fermi surface appears to be consistent with that predicted by band structure calculations, although a

complete characterization of the band structure is rendered difficult by the existence of surface states, which dominate surface-sensitive experiments such as tunneling and photoemission. The correspondence between the surface states and electronic states in the bulk is not yet established.

Complementary information on the chain states comes from penetration depth anisotropy measurements[11, 12] which indicate that the chains are superconducting below the bulk critical temperature T_c , and have a substantial superfluid density. Because the chains and CuO_2 planes are structurally different, the apparent similarity of their superconducting states, as measured by the penetration depth, was puzzling for many years. The chains, being far from half-filled, should not have an intrinsic pairing interaction capable of producing high critical temperatures. A more likely scenario is that the chains derive their superconductivity from proximity coupling to the CuO_2 planes.[13] Calculations showed that proximity models for chain superconductivity introduce small energy scales related to the induced gap in the chains. To date, these small scales have not been observed in penetration depth measurements.[14] It was later shown[15] that the smallest energy scale, which is relevant to low temperature measurements, comes from a subset of chain-derived electronic states that are weakly hybridized with the CuO_2 planes. Since these particular states have a predominantly 1D character, they are strongly affected by localization corrections due to chain disorder, and are therefore difficult to detect via the electrodynamic response.

Small energy scales have been seen in other experiments. For example, it has been found[16, 17] that the vortex cores in $\text{YBa}_2\text{Cu}_3\text{O}_{7-\delta}$, as measured by μSR experiments, are much larger at small magnetic fields B than expected from the measured upper critical field, and that the cores contract rapidly with increasing B below a crossover field B^* . This anomalous behaviour has been explained by the presence of CuO chains[18, 19], and it can be shown that $B^* \sim E_s^2$. It has also been suggested that a similar small energy scale seen in tunneling experiments[20, 21, 22] can be attributed to the chains.

In summary, we argue that there is reasonable evidence that the CuO chains in $\text{YBa}_2\text{Cu}_3\text{O}_{7-\delta}$ (a) are metallic, (b) are significantly hybridized with the CuO_2 planes, and (c) superconduct as a result of this hybridization. There remain many unresolved questions regarding the role of the chains, however. First, there are practical issues: neither the strength nor momentum-dependence of the chain-plane coupling have been established with any degree of certainty. Second, there are questions of fundamental interest: what are the properties of a weakly correlated 1D metal in close contact with a strongly-correlated electron liquid. Finally, there is the question of how the chains manifest themselves in various experiments. In some cases, for example transport anisotropy, the role played by the chains is intuitively obvious. However, in many cases, the effects of the chains are not *a priori* obvious, as in the case of the vortex core contraction mentioned above.

In this work, we examine the effects of chains on the local density of states (LDOS) $\rho(\mathbf{r}, \omega)$ in the vortex state of $\text{YBa}_2\text{Cu}_3\text{O}_7$. Experiments have found that the electronic structure of vortices in $\text{YBa}_2\text{Cu}_3\text{O}_{7-\delta}$ is different from other HTS[23] and

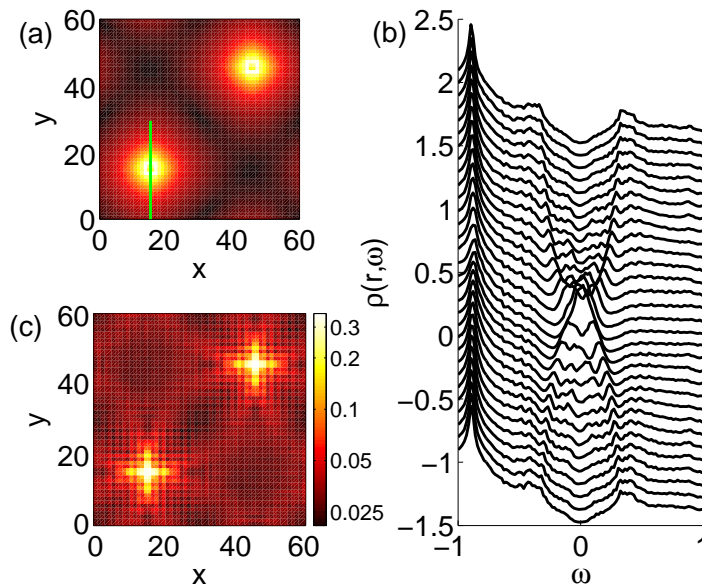


Figure 1. Electronic structure near the vortex core for a single tetragonal layer with a d -wave superconducting order parameter. (a) Magnitude of the current density $|\mathbf{j}(\mathbf{r})|$ as a function of position. The figure shows a pair of vortices belonging to a square lattice whose axes are rotated 45° relative to the crystalline axes (which are parallel to the figure axes). (b) Local density of states at a series of positions along the line drawn through the lower vortex core in (a). Note that the nondispersing peak at $\omega = -0.9$ is a van Hove singularity associated with the band structure. Far from the vortex core, the d -wave order parameter is $|\Delta| = 0.38$. (c) The LDOS $\rho(\mathbf{r}, \varepsilon_F)$ is shown as a function of position near a single vortex core. Note the logarithmic scale. Here and throughout the Fermi energy is $\varepsilon_F = 0$.

from theoretical calculations[24, 25]. Theory predicts that, for a single superconducting layer with a d -wave order parameter, there should be a peak in the LDOS at the vortex core centre (a “zero bias conduction peak” or ZBCP), and that as one moves away from the core, the peak splits and disperses towards higher energies, eventually merging with the coherence peaks far from the vortex core. This behaviour is illustrated in Figure 1, where the results of a calculation performed for a single-layer version of the model used in this work are shown.

Experimentally, the situation is rather different. The ZBCP at the vortex core is absent, and a pair of finite-energy peaks at $\omega \approx \pm 5$ meV are present instead. Furthermore, unlike the calculations, these peaks do not shift significantly as one moves away from the vortex core. It is possible that these peaks have the same origin as peaks measured in zero-field tunneling experiments, but this is not established.

In this work we ask two questions: (i) what are the signatures of the chains in the vortex structure within the proximity model and (ii) to what extent can the proximity model explain the existing experiments?

2. Method

Since the technical details of the calculation have been given in [19], we only give a summary of the main ideas here. The plane-chain model is made up of a single bilayer consisting of a tetragonal 2D plane layer (representing a CuO₂ layer) and a layer of 1D chains (representing a CuO layer). The layers are connected by single electron hopping, so that the plane and chain bands hybridize to form new bands. These bands have either predominantly plane or chain character, and we refer to them as plane-derived or chain-derived respectively. The chain layer is represented by a tight binding Hamiltonian with a single orbital per unit cell. In band structure calculations, this orbital is a linear combination of the chain Cu_{*d*_{*z*²-*y*²}} and O_{*p*_{*y*}} orbitals.[1] The CuO₂ band structure is also represented by a tight binding model with a single orbital per unit cell. In this case, the orbital represents a singlet state involving the Cu_{*d*_{*z*²-*y*²}} and O_{*p*_{*(x,y)*}} orbitals.[26].

There is a pairing interaction in the plane layer leading to *d*-wave superconductivity, but the chain layer is intrinsically normal. Nonetheless, the chain superconducts because of the the proximity effect; single electron hopping between the plane and chain layers induces a gap in the chains. One important feature of the proximity model is that the induced gap in the chains does not share the *d*-wave symmetry of the plane layer[15]. This is because the chain dispersion is quasi-1D, and the **k**-dependence of the excitation gap depends on the symmetry of both the order parameter and the underlying band.

We define coordinates *x*, *y*, and *z* which are aligned with the crystalline axes *a*, *b*, and *c* respectively, and consider a magnetic field aligned with the *c*-axis. The screening currents, therefore, circulate within the plane and chain layers. It is for this configuration that the vortex core contraction is seen in μ SR experiments,[16] and that STM experiments are performed.

The Hamiltonian is

$$\hat{H} = \hat{H}_1 + \hat{H}_2 + \hat{H}_\perp. \quad (1)$$

where \hat{H}_1 is the Hamiltonian for the isolated plane, \hat{H}_2 the Hamiltonian for the isolated chains, and \hat{H}_\perp the single-electron hopping term that couples the two layers. For comparison, we also consider a single-layer model described by \hat{H}_1 alone. We have

$$\begin{aligned} \hat{H}_1 = & \sum_{ij\sigma} \tilde{t}_{1ij} c_{1\sigma}^\dagger(\mathbf{r}_i) c_{1\sigma}(\mathbf{r}_j) + \sum_{ij} [\Delta_{ij} c_{1\uparrow}^\dagger(\mathbf{r}_i) c_{1\downarrow}^\dagger(\mathbf{r}_j) \\ & + \Delta_{ij}^* c_{1\downarrow}(\mathbf{r}_j) c_{1\uparrow}(\mathbf{r}_i)], \end{aligned} \quad (2)$$

where $c_{1\sigma}(\mathbf{r}_i)$ is the annihilation operator for an electron in the plane on site *i* with spin σ , and position $\mathbf{r}_i = (x_i, y_i)$, \tilde{t}_{1ij} are hopping matrix elements, and Δ_{ij} are superconducting pair energies. The subscripts “1” and “2” refer to the plane and chain layers respectively. The hopping matrix element \tilde{t}_{1ij} between sites *i* and *j* includes the effects of the magnetic field via

$$\tilde{t}_{1ij} = t_{1ij} \exp \left[-i \frac{e}{\hbar c} \int_{\mathbf{r}_j}^{\mathbf{r}_i} \mathbf{dr} \cdot \mathbf{A}(\mathbf{r}) \right]$$

$$= t_{1ij} \exp \left[i\alpha \frac{y_i + y_j}{2} (x_i - x_j) \right], \quad (3)$$

where t_{1ij} are the zero-field matrix elements, $\mathbf{A}(\mathbf{r}_i) = -B_0 y_i \hat{\mathbf{x}}$ is the static magnetic vector potential, B_0 is the uniform applied magnetic field, and $\alpha = eB_0/\hbar c$.

We take a square tight-binding lattice with hopping up to second-nearest neighbours. The matrix elements in zero magnetic field are $t_{1ii} = t_{1,0}$, $t_{1\langle i,j \rangle} = t_{1,\text{nn}}$, and $t_{1\langle\langle i,j \rangle\rangle} = t_{1,\text{nnn}}$, where $\langle i,j \rangle$ and $\langle\langle i,j \rangle\rangle$ refer to nearest and next-nearest neighbours respectively. When $B = 0$, the dispersion is $\epsilon_1(\mathbf{k}) = t_{1,0} + 2t_{1,\text{nn}}(\cos k_x + \cos k_y) + 4t_{1,\text{nnn}} \cos k_x \cos k_y$.

The order parameter for superconductivity is denoted Δ_{ij} , where i and j denote sites on the lattice. The order parameter is determined self-consistently using a nearest-neighbour attractive interaction of magnitude V . Then,

$$\Delta_{ij} = -\frac{V}{2} \langle c_{1\downarrow}(\mathbf{r}_j) c_{1\uparrow}(\mathbf{r}_i) + c_{1\downarrow}(\mathbf{r}_i) c_{1\uparrow}(\mathbf{r}_j) \rangle \delta_{\langle i,j \rangle}. \quad (4)$$

The d-wave component, defined by $\Delta(\mathbf{r}_i) = \sum_j (-1)^{y_i - y_j} \Delta_{ij}$, is the dominant component of the order parameter.

The Hamiltonian for the chain layer is

$$H_2 = \sum_{ij\sigma} t_{2ij} c_{2\sigma}^\dagger(\mathbf{r}_i) c_{2\sigma}(\mathbf{r}_j) \quad (5)$$

where $t_{2ii} = t_{2,0}$ and $t_{2ij} = t_{2,\text{nn}}$ for i and j nearest-neighbour sites belonging to the same chain. The matrix elements are unchanged by the magnetic field because of the choice of gauge. When $B = 0$, the chain dispersion is $\epsilon_2(\mathbf{k}) = t_{2,0} + 2t_{2,\text{nn}} \cos k_y$.

The term describing the interlayer hopping is

$$H_\perp = t_\perp \sum_{i\sigma} [c_{1\sigma}^\dagger(\mathbf{r}_i) c_{2\sigma}(\mathbf{r}_i) + c_{2\sigma}^\dagger(\mathbf{r}_i) c_{1\sigma}(\mathbf{r}_i)], \quad (6)$$

which mixes the chain and plane wavefunctions.

The model parameters used in this work are $\{t_{1,0}, t_{1,\text{nn}}, t_{1,\text{nnn}}, t_{2,0}, t_{2,\text{nn}}, t_\perp\} = \{1.0, -1.0, 0.45, 2.4, -2.0, 0.6\}$, and the pairing interaction is $V = 1.3$. With these definitions, we have taken the magnitude of the nearest-neighbour hopping (i.e. $|t_{1,\text{nn}}|$) as the scale of energy. This will be our energy scale throughout this work, and a rough comparison to experiments may be made by taking $t_{1,\text{nn}} \sim 100$ meV. However, we emphasize that quantitative comparisons to experiments are not possible because the model parameters are chosen for numerical convenience (i.e. such that the energy scale E_s associated with chain superconductivity is easily resolved), rather than to reproduce the $\text{YBa}_2\text{Cu}_3\text{O}_{7-\delta}$ band structure accurately.

There is a quasi-periodicity which allows us to define an $L_x \times L_y$ magnetic supercell containing $N = L_x L_y / a_0^2$ atomic lattice sites (a_0 is the lattice constant) and enclosing two superconducting flux quanta (i.e. two vortices), where the superconducting flux quantum is $\Phi_0 \equiv hc/2e$. The magnetic field is therefore $B = 2\Phi_0 / L_x L_y$. In order to obtain low magnetic fields, we need large values of L_x and L_y . Unless otherwise stated, all results shown in this paper are for a $60 \times 60 \times N_z$ -site supercell ($N_z = 1, 2$) corresponding to $B = 2\Phi_0 / 3600$. For this case, we sum over $5^2 = 25$ \mathbf{K} -vectors, which

is formally equivalent to studying a system of 50 vortices on a $300 \times 300 \times 2$ site lattice. Taking a unit cell size of $a_0 = 4 \text{ \AA}$, this corresponds to $B = 7 \text{ T}$. While this is a strong field for $\text{YBa}_2\text{Cu}_3\text{O}_{7-\delta}$, we have chosen the model parameters such that this is in the low-field limit of the proximity model (i.e. chain superconductivity is not quenched at this field).

The details of the transformation to Bloch states are given in [19]. Here, we simply mention that our self-consistent calculations proceed in several steps. First, we diagonalize the Hamiltonian to generate a set of eigenenergies $E_{i,\mathbf{K}}$ and wavefunctions $\Psi_{\alpha,\mathbf{K}}(n, \sigma, \mathbf{r})$ where \mathbf{K} are the supercell wavevectors, $\alpha \in (1, 2N)$ (the factor of two is for spin) is a quantum number labelling the eigenenergies for each \mathbf{K} , $n = 1, 2$ refers to the layer, and \mathbf{r} to sites within each layer. Note that a Bogolyubov transformation has been made, such that the spin index refers to spin-up electrons with wavevector \mathbf{K} ($\sigma = \uparrow$) or spin-down holes with wavevector $-\mathbf{K}$ ($\sigma = \downarrow$). The second step is to calculate the Fourier-transformed order parameter $\Delta_{ij}(\mathbf{K})$ from the wavefunctions. This new order parameter is inserted into the Hamiltonian, and a new set of eigenfunctions and energies is calculated. The iterative process terminates when the largest difference between the input and output values of $\Delta_{ij}(\mathbf{K})$ is less than 10^{-3} .

We present results for two observables in this work. The LDOS at energy ω in layer n is

$$\begin{aligned} \rho_n(\mathbf{r}, \omega) = & \frac{1}{N_k} \sum_{\mathbf{K}} \sum_{\alpha=1}^{2N} [|\Psi_{\alpha,\mathbf{K}}(n, \uparrow, \mathbf{r})|^2 \delta(\omega - E_{\alpha,\mathbf{K}}) \\ & + |\Psi_{\alpha,\mathbf{K}}(n, \downarrow, \mathbf{r})|^2 \delta(\omega + E_{\alpha,\mathbf{K}})], \end{aligned} \quad (7)$$

and the total density of states (DOS) is $\rho(\omega) = N^{-1} \sum_n \sum_{\mathbf{r}} \rho_n(\mathbf{r}, \omega)$ where N is the total number of sites in the lattice. The second observable is the 2D current density in layer n , denoted by $\mathbf{j}_n(\mathbf{r}) = (j_{n,x}(\mathbf{r}), j_{n,y}(\mathbf{r}))$ with

$$\begin{aligned} j_{n,x}(\mathbf{r}_i) = & \frac{-e}{2\hbar a_0} \text{Im} \frac{1}{N_k} \sum_{\mathbf{K}} \sum_{\alpha=1}^{2N} f(E_{\alpha,\mathbf{K}}) \\ & \times \frac{1}{2} \sum_{\pm} [\tilde{t}_{n,ij}(\mathbf{K}) \Psi_{\alpha,\mathbf{K}}^*(n, \uparrow, \mathbf{r}_i) \Psi_{\alpha,\mathbf{K}}(n, \uparrow, \mathbf{r}_i \pm a_0 \hat{\mathbf{x}}) \\ & - \tilde{t}_{ij}(-\mathbf{K}) \Psi_{\alpha,\mathbf{K}}(n, \downarrow, \mathbf{r}_i) \Psi_{\alpha,\mathbf{K}}^*(n, \downarrow, \mathbf{r}_i \pm a_0 \hat{\mathbf{x}})], \end{aligned} \quad (8)$$

and a similar expression for $j_{n,y}(\mathbf{r}_i)$. Note that the layer index n is omitted when we present quantities for the single-layer model.

3. Results and Discussion

The LDOS is shown in Figure 1 for a model consisting of a single tetragonal plane. This case is well-studied, and we include it here as a point of comparison for later calculations. In this figure, one sees a ZBCP at the vortex core. Away from the vortex core, the ZBCP splits into two peaks which disperse away from the Fermi energy ε_F as the distance to the core increases, eventually merging with the coherence peaks at

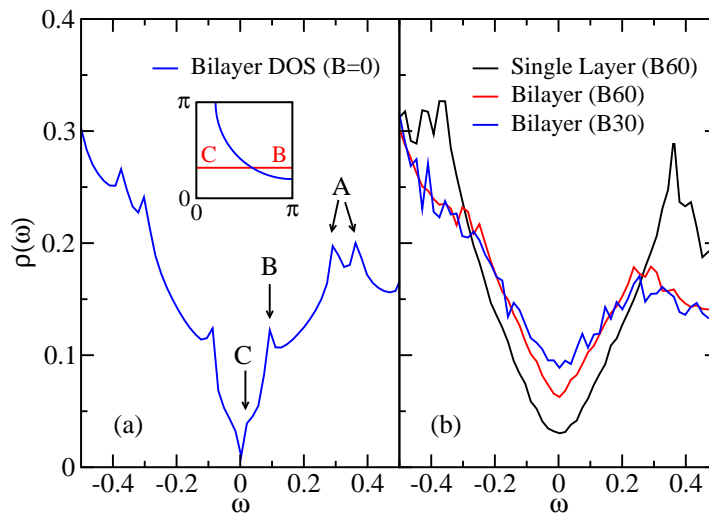


Figure 2. Superconducting density of states. (a) Spatially-averaged density of states in zero magnetic field for the bilayer model. The superconducting coherence peaks for the 2D plane are split by plane-chain coupling (A), while there are two distinct energy scales (B and C) associated with the induced gap in the chains. The inset shows a sketch of the chain (red) and plane (blue) Fermi surfaces. The portions of the chain Fermi surface contributing to the DOS at the energies B and C are indicated. (b) The effect of magnetic field on the spatially-averaged DOS. The field strengths are $B = 2\Phi_0/60^2$ (B60) and $B = 2\Phi_0/30^2$ (B30). The latter results are calculated using a $30 \times 30 \times 2$ lattice with 15^2 supercell \mathbf{K} -points.

$\omega = \pm E_L$. This is the behaviour predicted for isolated vortices in both s -[27] and d -wave[25, 24, 28] superconductors. For an isolated vortex in an s -wave superconductor, quasiparticle eigenstates have a well-defined angular momentum, and it was shown that peaks at different distances from the core correspond to different angular momentum eigenstates. Sufficiently near the core, both the peak energy and distance to the core are linearly proportional to the angular momentum.[29] As we will show, this relationship between angular momentum and the peak energy is relevant to the electronic structure of CuO chains in the vortex state.

We remark that, although dispersing peaks have been observed experimentally in the s -wave superconductor NbSe₂[30], they have not been seen in either YBa₂Cu₃O_{7- δ} or Bi₂Sr₂CaCu₂O₈. [23] A number of strong-correlation-related mechanisms have been proposed for the absence of the ZBCP[23], and it is known that disorder can suppress the ZBCP[23]. Furthermore, it is possible that nontrivial tunneling matrix elements can significantly alter the LDOS.[31] At present, the reason for the lack of a ZBCP in the HTS has not been resolved.

The spatial dependence of the LDOS at the Fermi energy, $\rho(\mathbf{r}, \varepsilon_F)$, is plotted in Figure 1(c). A logarithmic plot is used to emphasize the long-range tails extending from the vortex core. These are a signature of BCS-like d -wave superconductivity[25] and, like the ZBCP, have not been seen experimentally. Again, the reason for this is not clear.

In Figure 2, we compare the spatially-averaged density of states for three different cases: the bilayer model in zero magnetic field, and the single-layer and bilayer models for $B \neq 0$. This figure shows that the DOS for the bilayer model has a relatively complicated structure when $B = 0$, with four distinct energy scales (see [15] for a complete discussion). First, the coherence peaks associated with plane superconductivity are split by chain-plane coupling (A). A similar splitting has been observed in STM experiments[22]. We identify the lower-energy of the two coherence peaks as the “large gap” E_L . Because the chains act as pair-breakers, E_L is slightly smaller than the gap in the single-layer model. Next, there are two gap energy scales associated with induced superconductivity in the chains. The larger of these (B) comes from the region of the chain-derived Fermi surface nearest $(\pi, 0)$ in the Brillouin zone. Here, the energetic proximity of the chain and plane bands leads to a large hybridization of their wavefunctions and a relatively large induced gap. We believe that this energy scale, denoted E_s , is the small gap that has been seen in STM experiments in zero field. The smallest energy scale (C) is associated with superconductivity on the portion of the chain Fermi surface nearest the Brillouin zone centre. This gap is wiped out by small amounts of disorder or thermal broadening, and the proximity model therefore predicts a finite residual density of states at the Fermi energy, in accordance with tunneling experiments.[20, 21, 22]

The finite-field DOS is shown in Figure 2(b). The field washes out the distinct energy scales; however, E_s shows up in the field-dependence of the DOS. Compared with the single-layer model, $\rho(\varepsilon_F)$ for the bilayer model is a strong function of B for $B < B^*$, where $B^* \sim E_s^2$ [19] is the crossover field mentioned above. For $B > B^*$, $\rho(\varepsilon_F)$ varies at a similar rate with B in both the single-layer and bilayer models. Similar behaviour has been predicted in an anisotropic single-band model for $\text{YBa}_2\text{Cu}_3\text{O}_{7-\delta}$ [32]. In the bilayer model studied here, B^* is the magnetic field above which the vortex cores in the chains begin to overlap. From the perspective of the chains, there are therefore distinct low- ($B < B^*$) and high- ($B > B^*$) field regimes. Experimentally, $B^* \approx 1$ T in $\text{YBa}_2\text{Cu}_3\text{O}_{6.95}$. Because we have chosen a large value for the chain-plane coupling, the data shown here for the $60 \times 60 \times 2$ lattices belong to the regime $B < B^*$.

The LDOS for the bilayer is shown along a series of cuts through the vortex along the $(1, 0)$ direction in Figure 3, the $(1, 1)$ direction in Figure 4, and the $(0, 1)$ direction in Figure 5. The cuts are illustrated in Figure 3(d). There are three sources of anisotropy which contribute to differences in $\rho_n(\mathbf{r}, \omega)$ along the three directions. First, the d -wave order parameter vanishes for quasiparticles travelling in the $(1, \pm 1)$ directions and obtains its maximum along the $(1, 0)$ and $(0, 1)$ directions. Second, the shortest path between vortices lies along the $(1, \pm 1)$ directions. Third, the chains run parallel to the $(0, 1)$ direction. We can separate the third factor from the first two by comparing our bilayer results with those for the single-layer model.

First, we consider the cut along the $(1, 0)$ direction (Figure 3). The LDOS in the plane layer exhibits one notable difference from the single layer case shown in Figure 1: the ZBCP splits into a quartet, instead of a pair, of dispersing peaks as one moves away

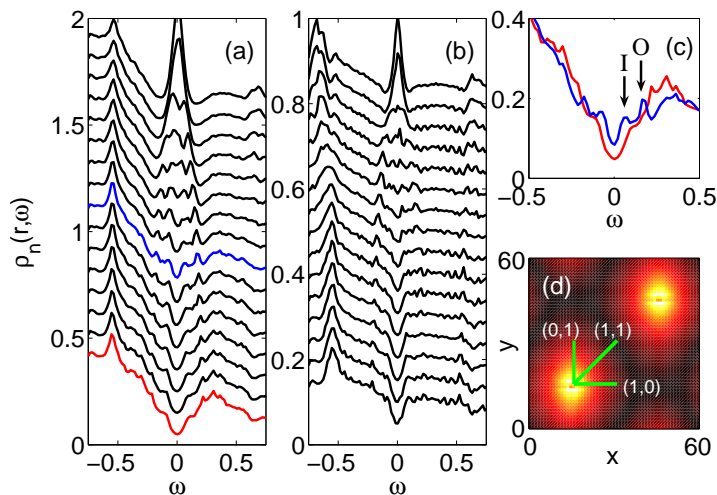


Figure 3. Local density of states in the bilayer model. (a) The LDOS $\rho_1(\mathbf{r}, \omega)$ in the 2D plane at positions between the vortex core (top curve) and the edge of the vortex (bottom curve). Curves are offset for clarity. Positions are taken along the (1,0) cut shown in (d). (b) $\rho_2(\mathbf{r}, \omega)$ in the 1D chain layer at identical positions to (a). (c) Two of the LDOS curves from (a) are compared, showing the dispersion of the inner (I) and outer (O) peaks. Curve colours are the same as in (a). (d) Spatial dependence of the current density $|\mathbf{j}_1(\mathbf{r})|$ in the plane layer for a pair of vortices. The lines indicate the cuts along which LDOS curves are displayed in this figure [(1,0)], Figure 4 [(1,1)] and Figure 5 [(0,1)]. Note that the (0,1) and (1,0) cuts are parallel and perpendicular to the chains respectively.

from the vortex core. The outer peaks asymptotically approach E_L at large distances from the vortex core, while the inner peaks asymptotically approach E_s . It appears as if the presence of two superconducting energy scales leads to the formation of two distinct sets of dispersing quasi-bound resonances.

The LDOS curves shown in Figure 3(b) come from different chains at increasing distances from the vortex core. As in the plane, there is a ZBCP at the vortex core. The splitting of the ZBCP that is readily apparent in the plane layer is also present, although difficult to resolve, in the chain layer. The LDOS curves far from the vortex core closely resemble the DOS for the chains when $B = 0$: there is a pronounced suppression of the DOS for $|\omega| < E_s$, a large residual DOS at $\omega = \varepsilon_F$, and there are weak remnants of the coherence peaks at E_L coming from the superconductivity in the planes.

The LDOS is shown along the (1,1) direction in Figure 4. In both the single-layer and bilayer models, the peaks disperse more quickly along the (1,1) direction than along the (1,0) direction. Furthermore, in the case of the bilayer model, the inner peaks are weak and difficult to resolve.

When the cut is taken along the (0,1) direction (Figure 5), the single layer model gives the same LDOS curves as in the (1,0) direction, as required by the fourfold symmetry of the lattice. The bilayer model, however, is qualitatively different along the (0,1) and (1,0) cuts. In the plane layer, there are a pair of dispersing peaks

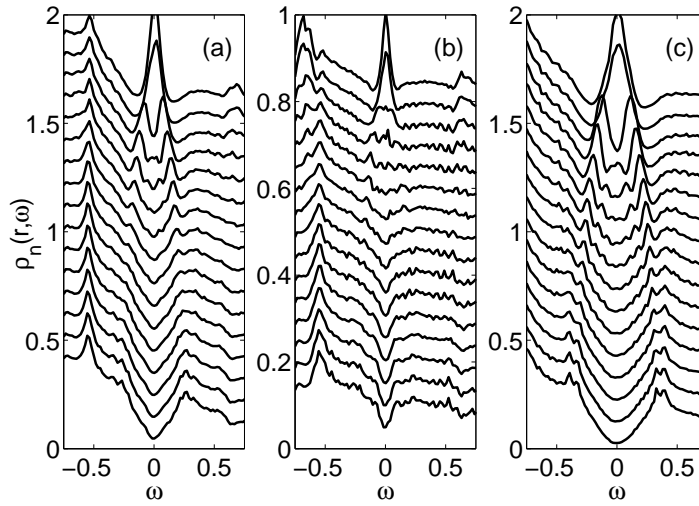


Figure 4. Local density of states in the bilayer model for the (a) plane and (b) chain layers. Cuts are taken along the (1, 1) direction, illustrated in Figure 3(d), with the vortex core corresponding to the top curve. The LDOS is also shown in (c) for the single-layer model.

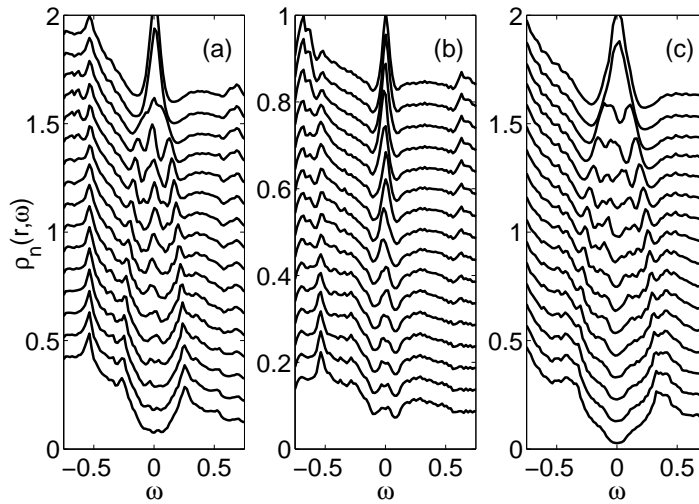


Figure 5. Local density of states in the bilayer model for the (a) plane and (b) chain layers. Cuts are taken along the (0, 1) direction, illustrated in Figure 3(d), with the vortex core corresponding to the top curve. The LDOS is also shown in (c) for the single-layer model.

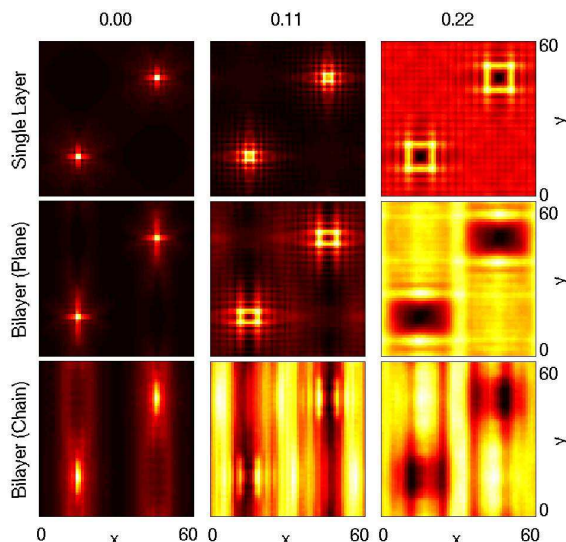


Figure 6. LDOS maps for two vortices on a $60 \times 60 \times N_z$ lattice. Figures show $\rho_n(\mathbf{r}, \omega)$ as a function of \mathbf{r} for the single-layer ($N_z = 1$; top row), and bilayer model ($N_z = 2$; middle and bottom rows). Each column corresponds to a different value of ω , indicated at the top of the column.

that asymptotically approach $\pm E_L$ at large distances from the vortex core. These peaks correspond to the outer peaks found along the $(1, 0)$ direction. In contrast, the inner peaks that are seen along the $(1, 0)$ direction are absent here. Instead, there is a pronounced ZBCP that extends ~ 10 unit cells from the vortex core along the $(0, 1)$ direction. The ZBCP is particularly pronounced in the chain layer, where extends a longer distance than in the plane layer. Closer examination reveals a very slight splitting of the peak at large distances. For reasons discussed below, we believe that this splitting occurs because chain-plane coupling makes the chain-derived states weakly 2D.

For comparison, the spatial maps of $\rho_n(\mathbf{r}, \omega)$ are shown at three different values of ω in Figure 6. This figure provides a different perspective on the results presented in the preceding discussion. We begin with the plots for $\omega = \varepsilon_F$. The single-layer model exhibits a fourfold symmetry, as expected. The ZBCP appears as the bright cross in the middle of each vortex core, and disappears away from core, where the peaks disperse to higher energies. In the bilayer model, we can clearly see that the LDOS in the plane, $\rho_1(\mathbf{r}, \varepsilon_F)$, is orthorhombically distorted and has long tails along the chain direction. In the chain layer, the vortex core is even more anisotropic; the extent of the core states along the a -axis is similar to that in the plane layer, but the extent along the b -axis is determined by the coherence length in the chains, $\xi_c = \hbar v_{F,c} / \pi E_s \approx 10a_0$, where $v_{F,c}$ is the chain Fermi velocity.

At the two larger values of ω , the LDOS shows a vortex core that appears to expand with increasing ω . This is because the apparent border of the core is determined by the positions of the dispersing peaks at that value of ω . As discussed earlier, the position and

energy of these peaks are approximately linearly related. The most noticeable difference between the single-layer and bilayer models is the orthorhombic distortion of the vortex core in the bilayer model, not present in the single-layer calculation. The single-layer model exhibits the fourfold “star” shape, first described in [25], while the LDOS in the bilayer plane is stretched along the a -axis, perpendicular to the chains. We note that STM experiments in $\text{YBa}_2\text{Cu}_3\text{O}_{7-\delta}$ found a similar stretching of the cores along the a -axis, with a ratio of ~ 1.5 between major and minor axes.[23] Although our results are suggestive, it is premature to declare the chains to be the underlying mechanism for this anisotropy, especially given the number of unresolved discrepancies between theory and experiment. We return to this point below.

We can construct a qualitative argument for the anisotropy between the $(1,0)$ and $(0,1)$ directions in the dispersion of the inner peaks. The fact that these peaks asymptotically approach E_s at large distances from the vortex core suggests that they are closely connected to superconductivity in the chain layer. We therefore consider the behaviour of quasiparticles travelling at the chain Fermi velocity $v_{F,c}$ within a chain a perpendicular distance r_\perp from the vortex core. Since the direction along which the quasiparticle travels does not change as it moves along the chain, the quasiparticle angular momentum is conserved and is $L_c = r_\perp v_{F,c}$. This is obviously an approximate statement since a quasiparticle, as a result of chain-plane hybridization, spends a fraction of its time in the plane layer where its trajectory is altered by the magnetic field. The linear relationship between r_\perp and L_c is therefore also approximate. However, it is sufficient to explain the anisotropy between $(1,0)$ and $(0,1)$ directions. We recall that in conventional superconductors there is a linear relationship between the angular momentum of a quasiparticle eigenstate and its energy.[29, 27] For the $(1,0)$ cut, r_\perp is equal to the distance r from the vortex core, L_c grows linearly with r , and the inner peaks are expected (by this argument) to disperse linearly with r . This prediction is consistent with the numerical results shown in Figure 3. On the other hand, $r_\perp = 0$ everywhere along the $(0,1)$ cut, since that cut follows along the chain that passes through the vortex core. We therefore have $L_c = 0$ everywhere along this cut, and the inner peaks remain at $\omega = \varepsilon_F$. Since the single-electron hopping between the chain and plane layers makes the chain-derived states weakly 2D, L_c is only approximately conserved along the length of the chain. We therefore expect a very weak dispersion of the peak energies along the $(0,1)$ direction. Again, this simple argument is consistent with numerical results, shown in Figure 5.

We finish this section with a brief discussion of the relevance of this work to experiments. There is a large body of literature attempting to explain STM experiments in HTS, both in zero magnetic field and in finite fields[23]. Existing theories are successful at reproducing broad qualitative features of the DOS spectrum, but generally fail to correctly predict quantitative details such as the spatial dependence of the LDOS near isolated impurities or vortex cores. The same appears to be true of the work discussed here: the proximity model is consistent with experiments indicating the existence of a small superconducting gap scale $E_s \approx 5$ meV but, as with previous

calculations, there is a discrepancy between the experiments and theory regarding the spatial dependence of the LDOS. Whether the failure to explain experiments is an experimental issue, or is due to unknown tunneling matrix element effects, surface states, or a failure of the basic mean-field model, is unclear at this stage.

Because of these uncertainties, we seek simple qualitative predictions stemming from the proximity model that might reveal something about the electronic structure of the vortex cores. We believe that one qualitative feature predicted by the proximity model, the existence of an anisotropy in the low energy LDOS between the $(1,0)$ and $(0,1)$ directions, should hold regardless of the details of the model. An experiment to measure such an anisotropy would establish whether E_s does, in fact, originate with the chains. In order to address this question, it will be necessary to perform experiments at strong fields where the vortex lattice is square.

4. Conclusions

We have studied the local density of states near a vortex core within a proximity model for $\text{YBa}_2\text{Cu}_3\text{O}_{7-\delta}$. This model incorporates both CuO_2 planes and CuO chains. The proximity model predicts that the CuO chains introduce a set of dispersing peaks in the LDOS, in addition to the peaks predicted for a single-layer superconductor. These peaks are associated with the small induced gap in the chain layer, and consequently have a strongly anisotropic dispersion. At $\omega = \varepsilon_F$, the LDOS is extended along the chain direction, but at $\omega > \varepsilon_F$, the vortex cores appear stretched along the a -axis.

Acknowledgments

This work was supported by NSERC of Canada. Calculations were performed using the High Performance Computing Virtual Laboratory (HPCVL).

References

- [1] O. K. Andersen, A. I. Liechtenstein, O. Jepsen, and F. Paulsen. LDA energy bands, low-energy hamiltonians, t' , t'' , $t_{\perp}(k)$, and J_{\perp} . *J. Phys. Chem. Solids*, 56:1573–1591, 1995.
- [2] T. A. Friedmann, M. W. Rabin, J. Giapintzakis, J. P. Rice, and D. M. Ginsberg. Direct measurement of the anisotropy of the resistivity in the a-b plane of twin-free, single-crystal, superconducting $\text{YBa}_2\text{Cu}_3\text{O}_{7-\delta}$. *Phys. Rev. B*, 42(10):6217–6221, Oct 1990.
- [3] S. J. Hagen, T. W. Jing, Z. Z. Wang, J. Horvath, and N. P. Ong. Out-of-plane conductivity in single-crystal $\text{YBa}_2\text{Cu}_3\text{O}_7$. *Phys. Rev. B*, 37(13):7928–7931, May 1988.
- [4] K. Takenaka, K. Mizuhashi, H. Takagi, and S. Uchida. Interplane charge transport in $\text{YBa}_2\text{Cu}_3\text{O}_{7-y}$: Spin-gap effect on in-plane and out-of-plane resistivity. *Phys. Rev. B*, 50(9):6534–6537, Sep 1994.
- [5] C. C. Homes, S. V. Dordevic, D. A. Bonn, Ruixing Liang, W. N. Hardy, and T. Timusk. Coherence, incoherence, and scaling along the c axis of $\text{YBa}_2\text{Cu}_3\text{O}_7$. *Phys. Rev. B*, 71(18):184515, 2005.
- [6] H. L. Edwards, D. J. Derro, A. L. Barr, J. T. Markert, and A. L. de Lozanne. Spatially varying energy gap in the CuO chains of $\text{YBa}_2\text{Cu}_3\text{O}_{7-x}$ detected by scanning tunneling spectroscopy. *Phys. Rev. Lett.*, 75(7):1387–1390, Aug 1995.

- [7] D. J. Derro, E. W. Hudson, K. M. Lang, S. H. Pan, J. C. Davis, J. T. Markert, and A. L. de Lozanne. Nanoscale one-dimensional scattering resonances in the cuo chains of $\text{YBa}_2\text{Cu}_3\text{O}_{6+x}$. *Phys. Rev. Lett.*, 88(9):097002, Feb 2002.
- [8] D. H. Lu, D. L. Feng, N. P. Armitage, K. M. Shen, A. Damascelli, C. Kim, F. Ronning, Z.-X. Shen, D. A. Bonn, R. Liang, W. N. Hardy, A. I. Rykov, and S. Tajima. Superconducting gap and strong in-plane anisotropy in untwinned $\text{YBa}_2\text{Cu}_3\text{O}_{7-\delta}$. *Phys. Rev. Lett.*, 86(19):4370–4373, May 2001.
- [9] V. B. Zabolotnyy, S. V. Borisenko, A. A. Kordyuk, J. Geck, D. S. Inosov, A. Koitzsch, J. Fink, M. Knupfer, B. Büchner, S.-L. Drechsler, H. Berger, A. Erb, M. Lambacher, L. Patthey, V. Hinkov, and B. Keimer. Momentum and temperature dependence of renormalization effects in the high-temperature superconductor $\text{YBa}_2\text{Cu}_3\text{O}_{7-\delta}$. *Phys. Rev. B*, 76(6):064519, 2007.
- [10] K. Nakayama, T. Sato, K. Terashima, H. Matsui, T. Takahashi, M. Kubota, K. Ono, T. Nishizaki, Y. Takahashi, and N. Kobayashi. Bulk and surface low-energy excitations in $\text{YBa}_2\text{Cu}_3\text{O}_{7-\delta}$ studied by high-resolution angle-resolved photoemission spectroscopy. *Phys. Rev. B*, 75(1):014513, 2007.
- [11] Kuan Zhang, D. A. Bonn, S. Kamal, Ruixing Liang, D. J. Baar, W. N. Hardy, D. Basov, and T. Timusk. Measurement of the *ab* plane anisotropy of microwave surface impedance of untwinned $\text{YBa}_2\text{Cu}_3\text{O}_{6.95}$ single crystals. *Phys. Rev. Lett.*, 73(18):2484–2487, Oct 1994.
- [12] D. N. Basov, R. Liang, D. A. Bonn, W. N. Hardy, B. Dabrowski, M. Quijada, D. B. Tanner, J. P. Rice, D. M. Ginsberg, and T. Timusk. In-plane anisotropy of the penetration depth in $\text{YBa}_2\text{Cu}_3\text{O}_{7-x}$ and $\text{YBa}_2\text{Cu}_4\text{O}_8$ superconductors. *Phys. Rev. Lett.*, 74(4):598–601, Jan 1995.
- [13] W. A. Atkinson and J. P. Carbotte. Density of states of a layered s/n d-wave superconductor. *Phys. Rev. B*, 51(2):1161–1174, Jan 1995.
- [14] W. A. Atkinson and J. P. Carbotte. Effect of proximity coupling of chains and planes on the penetration-depth anisotropy in $\text{YBa}_2\text{Cu}_3\text{O}_7$. *Phys. Rev. B*, 52(14):10601–10609, Oct 1995.
- [15] W. A. Atkinson. Disorder and chain superconductivity in $\text{YBa}_2\text{Cu}_3\text{O}_{7-\delta}$. *Phys. Rev. B*, 59(5):3377–3380, Feb 1999.
- [16] J. E. Sonier, J. H. Brewer, R. F. Kiefl, G. D. Morris, R. I. Miller, D. A. Bonn, J. Chakhalian, R. H. Heffner, W. N. Hardy, and R. Liang. Field induced reduction of the low-temperature superfluid density in $\text{YBa}_2\text{Cu}_3\text{O}_{6.95}$. *Phys. Rev. Lett.*, 83(20):4156–4159, Nov 1999.
- [17] Jeff E Sonier. Investigations of the core structure of magnetic vortices in type-II superconductors using muon spin rotation. *Journal of Physics: Condensed Matter*, 16(40):S4499–S4513, 2004.
- [18] J. E. Sonier, S. A. Sabok-Sayr, F. D. Callaghan, C. V. Kaiser, V. Pacradouni, J. H. Brewer, S. L. Stubbs, W. N. Hardy, D. A. Bonn, R. Liang, and W. A. Atkinson. Hole-doping dependence of the magnetic penetration depth and vortex core size in $\text{YBa}_2\text{Cu}_3\text{O}_y$: Evidence for stripe correlations near (1/8) hole doping. *Phys. Rev. B*, 76(13):134518, 2007.
- [19] W. A. Atkinson and J. E. Sonier. Role of cuo chains in vortex core structure in $\text{YBa}_2\text{Cu}_3\text{O}_{7-\delta}$. *Phys. Rev. B*, 77(2):024514, 2008.
- [20] J. M. Valles, R. C. Dynes, A. M. Cucolo, M. Gurrutxaga, L. F. Schneemeyer, J. P. Garno, and J. V. Waszczak. Electron tunneling into single crystals of $\text{YBa}_2\text{Cu}_3\text{O}_{7-\delta}$. *Phys. Rev. B*, 44(21):11986–11996, Dec 1991.
- [21] N.-C. Yeh, C.-T. Chen, G. Hammerl, J. Mannhart, A. Schmehl, C. W. Schneider, R. R. Schulz, S. Tajima, K. Yoshida, D. Garrigus, and M. Strasik. Evidence of doping-dependent pairing symmetry in cuprate superconductors. *Phys. Rev. Lett.*, 87(8):087003, Aug 2001.
- [22] J. H. Ngai, W. A. Atkinson, and J. Y. T. Wei. Tunneling spectroscopy of c-axis $\text{Y}_{1-x}\text{Ca}_x\text{Ba}_2\text{Cu}_3\text{O}_{7-\delta}$ thin-film superconductors. *Phys. Rev. Lett.*, 98(17):177003, 2007.
- [23] Øystein Fischer, Martin Kugler, Ivan Maggio-Aprile, Christophe Berthod, and Christoph Renner. Scanning tunneling spectroscopy of high-temperature superconductors. *Reviews of Modern Physics*, 79(1):353, 2007.
- [24] Yong Wang and A. H. MacDonald. Mixed-state quasiparticle spectrum for d-wave

- superconductors. *Phys. Rev. B*, 52(6):R3876–R3879, Aug 1995.
- [25] Nils Schopohl and Kazumi Maki. Quasiparticle spectrum around a vortex line in a d-wave superconductor. *Phys. Rev. B*, 52(1):490–493, Jul 1995.
- [26] FC Zhang, C Gros, TM Rice, and H Shiba. A renormalized hamiltonian approach to a resonant valence bond wavefunction. *Superconductor Science & Technology*, 1(1):36–46, 1988.
- [27] François Gygi and Michael Schlüter. Self-consistent electronic structure of a vortex line in a type-II superconductor. *Phys. Rev. B*, 43(10):7609–7621, Apr 1991.
- [28] M. Kato and K. Maki. Self-consistent solution for a single vortex in d-wave superconductors. *EPL (Europhysics Letters)*, 54(6):800–806, 2001.
- [29] C. Caroli, P. G. De Gennes, and J. Matricon. Bound fermion states on a vortex line in a type II superconductor. *Phys. Lett.*, 9:307–309, 1964.
- [30] H. F. Hess, R. B. Robinson, and J. V. Waszczak. Vortex-core structure observed with a scanning tunneling microscope. *Phys. Rev. Lett.*, 64(22):2711–2714, May 1990.
- [31] Congjun Wu, Tao Xiang, and Zhao-Bin Su. Absence of the zero bias peak in vortex tunneling spectra of high-temperature superconductors. *Phys. Rev. B*, 62(21):14427–14430, Dec 2000.
- [32] N. D. Whelan and J. P. Carbotte. Magnetic field as a probe of gap energy scales in $yba2cu3o7 - x$. *Phys. Rev. B*, 62(22):15221–15225, Dec 2000.